ICAS 2021 SHANG HAI
International Council of the Aeronautical Sciences
32nd Congress of the International Council of the Aeronautical Sciences
September 6-10, 2021
Pudong Shangri-La, Shanghai, China

NUMERICAL SIMULATION OF VARIABLE WINGSPAN EFFECTS ON A BIONIC FLAPPING WING

Rui Zhang[1], Wenqing Yang[1,2], Yuanbo Li[1] & Jiangxin Gao[1]

[1]School of Aeronautics, Northwestern Polytechnical University, Xi'an, 710072, P. R. China

[2]Research & Development Institute of Northwestern Polytechnical University in Shenzhen, Shenzhen, 518057, China

Abstract

Many large and medium-sized birds have the spanwise folding movement of wings in their flight, resulting in the wingspan become larger during the downstroke and smaller during the upstroke. We studied the aerodynamic characteristics of a flapping wing with variable wingspan based on computational fluid dynamics (CFD) method. Reynolds-Averaged Navier-Stokes (RANS) method is utilized to solve the simulation of the flapping wing with variable wingspan, and is compared with the results of wing with fixed wingspan which shares the same averaged area with the former one. The considered wing planform is a simple rectangular, and the kinematics of the flapping wing are simulated by using dynamic mesh method. The variable wingspan effects are investigated under different cases, including different kinematics of the flapping wing and other influence parameters, such as the angle of attack (AoA), the flight speed, and the flapping frequency. Aerodynamic characteristics and flow structures of these cases are analyzed, due to the variable wingspan effects, the lift of the flapping wing increased significantly in the whole flapping cycle, the thrust of the flapping wing increased during the downstroke but reduced during the upstroke. Both the averaged lift and thrust are increased, and the variable wingspan effects can improve the aerodynamic performance of the flapping wing.

Keywords: flapping wing, variable wingspan, aerodynamic performance, dynamic mesh

1. Introduction

Birds can frequently transfer flight status between maneuvering flight and low-speed cruise flight, because they can actively change the shape of their wings to adapt to different flight conditions. Micro air vehicles (MAVs) have become a hot research topic in the field of aviation, which fly at the regime of low Reynolds numbers flows. Flapping-wing micro air vehicles (FMAVs) are thought to have high aerodynamic efficiency at low Reynolds number, and have received extensive research attention. FMAVs have bionic appearance and flight mode, and can generate lift and thrust simultaneously by flapping wings, which has potential advantages compared with fixed-wing or rotor aircrafts especially in specific application aeras [1,2]. In recent years, many bionic aircrafts with variable wingspan have been developed, such as Bat Bot, LisHawk, PigeonBot [3-5], however, there is still a big gap between their flight performance and that of birds or bats. In terms of robustness, adaptability, flight envelop and maneuverability, bats and birds have more outstanding flight performance [6].

In order to improve the flight performance of FMAVs, researchers could learn the flight mechanism from their natural counterparts. The complex low-Reynolds-number unsteady aerodynamics in flapping flight poses challenges to researchers. The kinematics of wings during animal flight is quite complex, which could be decomposed into several degrees of freedom (DOFs) including flapping, sweeping, pitching, flexing in span etc. The unsteady aerodynamic mechanism of flapping wings and their dependency on wing kinematics are receiving extensively concentration [7]. To understand some basic mechanism of flapping wings, it has become widely acceptable to use flat plates as a simplified substitute for the study of unsteady characteristics [8-10]. Some conclusion has been

obtained through previous research, the twisting wing can enhance the time averaged lift and generate the thrust during both the downstroke and the upstroke, and the wing-cambering along the chordwise direction and the wing-bending along the spanwise direction can greatly increase the lift but change the mean drag slightly [11-13]. In this paper, we also choose the flat plate with a rectangular planform as our research object to investigate the aerodynamic mechanism of flapping wing with dynamic wingspan. The flapping wing with fixed wingspan and variable wingspan are simulated, and the aerodynamic characteristics and evolution of vortex structure between these two cases are compared and analyzed. To investigate the variable wingspan effect of aerodynamic performance of the flapping wing in more extensive flight condition, some parameters of flight condition are concerned, such as AoA, flight speed and the flapping frequency. We hope to further explore the potential of the variable wingspan effects of a flapping wing for improving the flight performance.

2. Model and method

2.1 Wing model and kinematics

In the present research, the wing is simplified as a rectangular plate with chord length c = 0.1 m, and the plate thickness is 0.02c. The wing has two DOFs, namely, the wing dynamically changes span while flapping, imitating the change of wingspan when birds performing flapping-wing flight.

The kinematics of the flapping wing are defined as:

$$\Psi(t)=\Psi_m \sin(2\pi f t) \tag{1}$$

$$s(t)=s_0(a+b\sin(2\pi f t+\varphi)) \tag{2}$$

where $\Psi(t)$ is the stroke angle respect to the horizon at time t, Ψ_m is the stroke amplitude, $s(t)$ is the wingspan at time t and s_0 is the initial wingspan, a, b are the stretching factors. The angular frequency of the motion is given as $\omega = 2\pi f$, with f the flapping frequency. Furthermore, φ is the phase difference between the flapping motion and changing wingspan motion.

When s_0 = 2.5c, a = 1, b = 0.2, the wingspan s changes between 2c to 3c. $\varphi = -\pi/2$, the wingspan reaches the maximum in the middle position of downstroke, and the minimum in the middle position of upstroke, as shown in Figure 1.

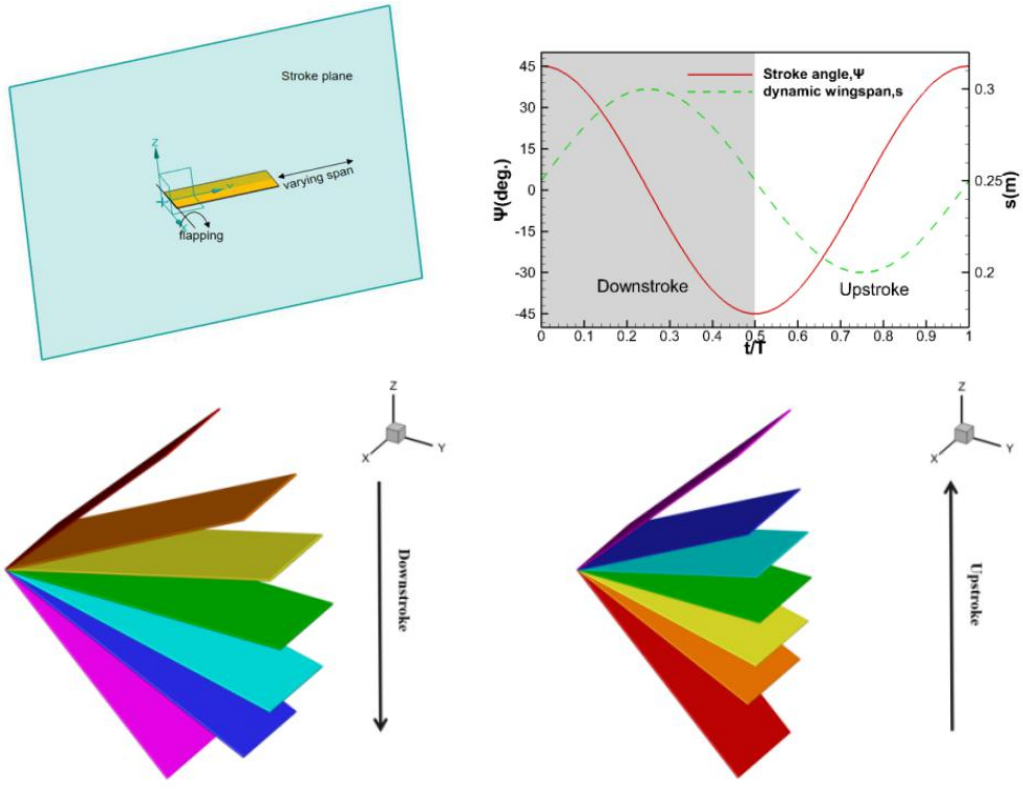

Figure 1 – Flapping wing model and kinematics (φ = −π/2).

2.2 Aerodynamic parameters

In this study, the aerodynamics of flapping wing with dynamic wingspan is analyzed, and the flow has obviously unsteady characteristics, thus two important non-dimentionalized parameters for unsteady flow analysis, Reynolds number (*Re*) and Strouhal number (*St*), are introduced. They are calculated by Eqs. (3) and (4) respectively:

$$\mathrm{Re} = \frac{\rho \mathrm{U}_0 c}{\mu} \tag{3}$$

$$St = \frac{f\mathrm{A}}{U_0} = \frac{f\mathrm{s}_0 \sin \Psi_\mathrm{m}}{U_0} \tag{4}$$

the Reynolds number represents the ratio of inertial forces to viscous forces, which is used to characterize different flow regimes, such as laminar, turbulent or transitional flow. In Eq. (3), U_0 is the flight speed, ρ denotes the density of the fluid and μ is the dynamic viscosity of the fluid. Strouhal number is the parameter for thrust generation, in which A is the wake width of the flapping wing. For this situation, assuming that the wake width is the amplitude of the middle wingspan, that is, $A = s_0 \sin \Psi_m$.

For a dynamic wingspan flapping wing with the time-dependent wing area, the lift coefficient (Cl_{inst}) and thrust coefficient (Ct_{inst}) in forward flight is defined as:

$$\mathrm{Cl}_{inst}(t) = \frac{\mathrm{L}(t)}{q_\infty S(t)} \tag{5}$$

$$\mathrm{Ct}_{inst}(t) = \frac{\mathrm{T}(t)}{q_\infty S(t)} \tag{6}$$

where $L(t)$ is the lift, $T(t)$ is the thrust, $q_\infty = 0.5\rho U_0^2$ is the dynamical pressure, and $S(t)$ is the instantaneous wing area. Theoretically, the effect of changing the wing area is removed in Cl_{inst} and Ct_{inst} since $S(t)$ is used for normalization.

To characterize the overall lift and thrust, the lift coefficient (Cl_0) and thrust coefficient (Ct_0) based on the time-averaged wing area S_0 is introduced, i.e.,

$$\mathrm{Cl}_0(t) = \frac{\mathrm{L}(t)}{q_\infty S_0} \tag{7}$$

$$\mathrm{Ct}_0(t) = \frac{\mathrm{T}(t)}{q_\infty S_0} \tag{8}$$

In order to show the lift enhancement by dynamic wingspan effects, increments of lift coefficient ΔCl_0 and ΔCl_{inst} are introduced:

$$\Delta\mathrm{Cl}_0(t) = \mathrm{Cl}_0(t) - \mathrm{Cl}_{flap}(t) \tag{9}$$

$$\Delta\mathrm{Cl}_{inst}(t) = \mathrm{Cl}_{inst}(t) - \mathrm{Cl}_{flap}(t) \tag{10}$$

where Cl_{flap} is the reference lift coefficient of the flapping wing with fixed wingspan, the fixed wingspan equals to the time-averaged wingspan of dynamic wingspan, namely, s=2.5c. Essentially, ΔCl_0 represents the lift increment generated by both the effect of changing the wing area and the effect of the flow structures altered by the dynamic wingspan, ΔCl_{inst} mainly represents the lift increment generated by the effect of the dynamic wingspan altered flow structures.

Just like the analysis of lift coefficient, increments of thrust coefficient ΔCt_0 and ΔCt_{inst} are introduced:

$$\Delta\mathrm{Ct}_0(t) = \mathrm{Ct}_0(t) - \mathrm{Ct}_{flap}(t) \tag{11}$$

$$\Delta \mathrm{Ct}_{inst}(t) = \mathrm{Ct}_{inst}(t) - \mathrm{Ct}_{flap}(t) \tag{12}$$

Since the actual velocity of incoming flow relative to the wing chord is the vector resultant of flight velocity and flapping induced velocity, as shown in Figure 2, the effective angle of attack α_{eff} is introduced:

$$\alpha_{eff} = \alpha_0 + \arctan\frac{-U_{flap}}{U_0} \tag{13}$$

where α_0 is the AoA of the wing without flapping, U_{flap} is the flapping wing induced velocity, $U_{flap} = \dot{\Psi}(t) \cdot s$.

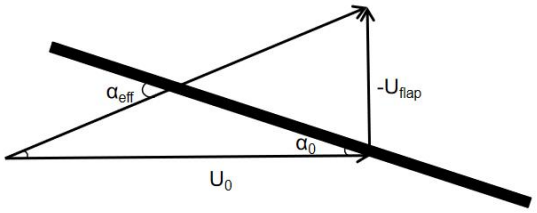

Figure 2 – Effetive angle of attack.

2.3 Numerical method and validation

The wing has two DOFs with large displacements, so the dynamic mesh method is used to realize the kinematics of the wing. The flapping motion of the wing can be realized by coordinate transformation, and the wingspan can be changed at the same time by the expansion coefficient f_l. The coordinate transformation is shown in Eqs. (14):

$$\begin{bmatrix} y' \\ z' \end{bmatrix} = \begin{bmatrix} \cos\Psi(t) & -\sin\Psi(t) \\ \sin\Psi(t) & \cos\Psi(t) \end{bmatrix} \bullet \begin{bmatrix} y - y_0 \\ z - z_0 \end{bmatrix} \bullet f_l + \begin{bmatrix} y_0 \\ z_0 \end{bmatrix} \tag{14}$$

where (y, z) is the original coordinates of the wing grid nodes, (y', z') is the time-dependent coordinates, (y_0, z_0) is the flapping pivot.

In this study, ANSYS Fluent has been used to perform the analysis of the time-dependent flow over flapping wing. RANS is utilized to investigate the aerodynamic characteristics. In the calculation of turbulent flow, the Shear Stress Transport (SST) k-ω turbulence model (two-equation model) has been used. The wing kinematics is imposed by defining the coordinate transformation in a User Defined Function (UDF). The calculation domain size is 62c×42c×21c to avoid wall interference. As shown in Figure 3, using structured grid in background zone to reduce grid quantity and improve computing efficiency. The unstructured mesh is used in the component zone to adapt to the large displacements of the wing and ensure the grid quality. The dimensionless wall distance is always such that y+ is equal or close to 1.

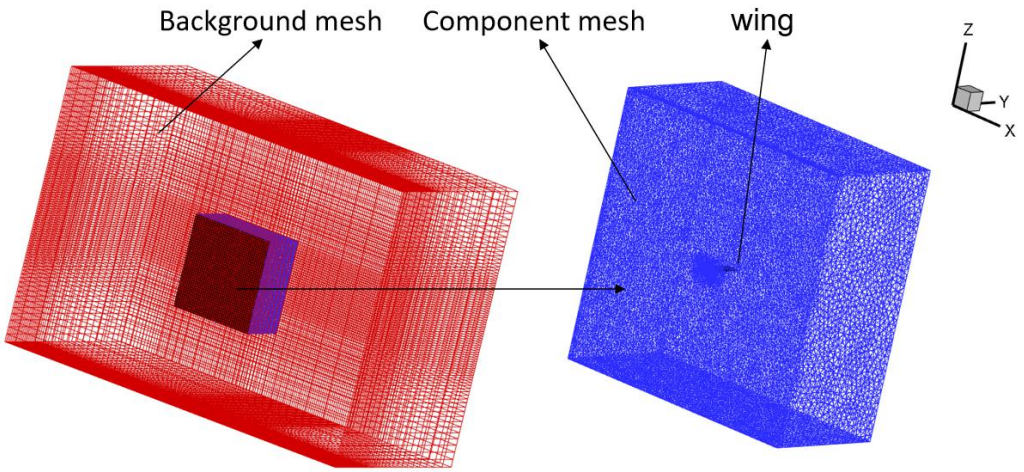

Figure 3 – Computational domain and overset mesh setup.

Validation of the CFD method is firstly implemented by an extended study on time accuracy of thrust forces generated by a NACA0012 rectangular wing with plunging motion. Computed thrust coefficient is compared with the experimental result by Heathcote [14] and computational result by LIU [15], as shown in Figure 4. It is seen that the case shows very reasonable agreement with the measured thrust coefficients.

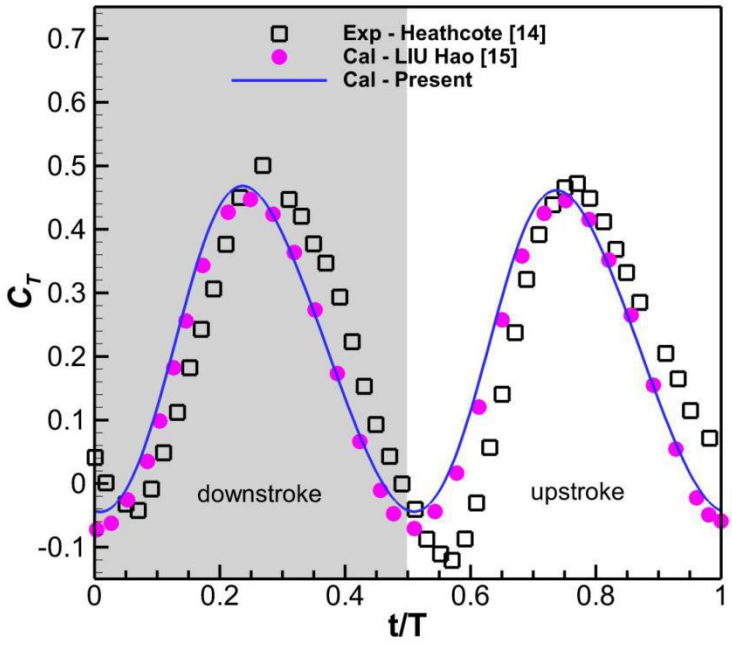

Figure 4 – Time course of thrust coefficients compared with previous research.

The mesh resolution and time step size of RANS method will affect the accuracy of numerical results. The detail of mesh resolution used for verification is listed in Table 1. After the third period, the calculated results tend to be stabilized, and the results is shown in Figure 5. After the verification of mesh resolution and time step size, the present numerical simulations on the flapping wing have been performed using the middle mesh resolution and 200 time-steps per period.

Table 1 Mesh resolution

Mesh resolution	Component mesh	Background mesh	Total mesh
coarse	672,462	438,265	1,110,727
middle	1,186,080	792,000	1,978,080
fine	2,217,758	1,285,200	3,502,958

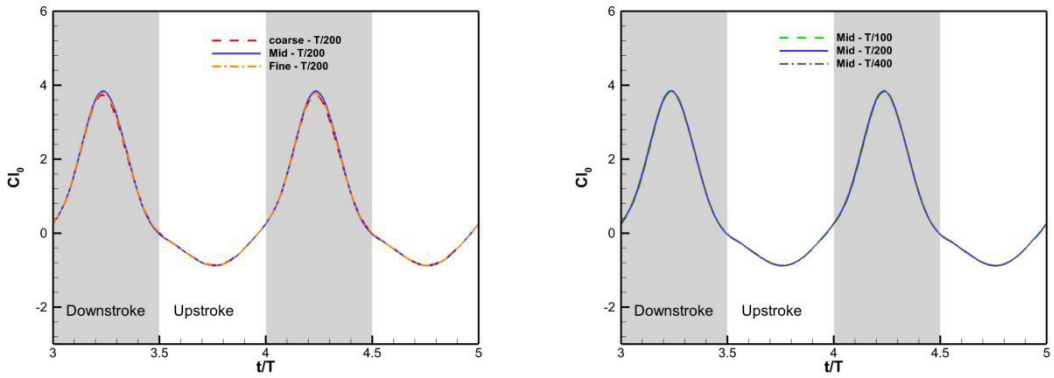

Figure 5 – The verification of mesh resolution and time step size.

3. Results and discussions

3.1 Variable wingspan effects

To investigate the variable wingspan effects, the aerodynamic characteristics and flow structures of the flapping wing with dynamic wingspan and fixed wingspan are simulated and analyzed. Both cases have the same boundary conditions, which were set to U_0 = 5m/s, f = 4Hz, Ψ_m=π/4, α_0=5°. Setting φ = −π/2 for the flapping wing with dynamic wingspan, and the wingspan reaches the maximum in the middle of downstroke, and the minimum in the middle of upstroke.

3.1.1 Aerodynamic characteristics

The time courses of lift coefficients are shown in Figure 6 (left), <V> means averaged variables. The overall variations of the lift coefficients are similar. The lift coefficients are larger during the downstroke, and reach the peak in the middle position, then decrease until the middle position of upstroke and reach the minimum. The averaged lift coefficient of flapping wing with dynamic wingspan nearly double compared with that of fixed wingspan. After removing the influence of the area, the averaged lift coefficient increased by 53.72%. It can be seen that the lift increment caused by the flow structures is slightly larger than that caused by the area effect.

The increments of lift coefficient are shown in Figure 6 (right), which are positive all the time. It can be seen that the area changes and flow structures change caused by dynamic wingspan have obviously enhanced the lift coefficient.

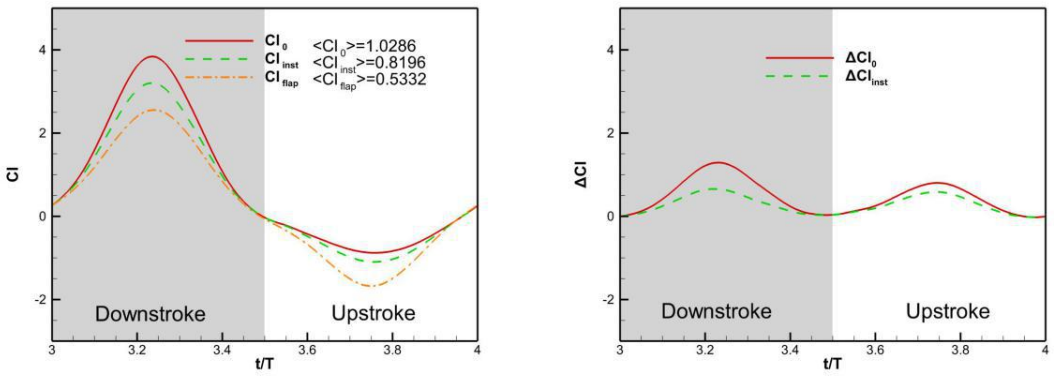

Figure 6 – Time courses of lift coefficient (left) and lift coefficient increments (right).

The time courses of thrust coefficient are shown in Figure 7 (left). The wing with fixed wingspan can produce positive thrust in most time of the flapping cycle, and the thrust is larger during the downstroke. The wing with dynamic wingspan produces larger thrust during the downstroke, but produces drag during the upstroke. In addition, the thrust coefficient Ct_0 is significantly larger than Ct_{inst} during the downstroke, while they are almost equal during the upstroke. The averaged thrust coefficient of flapping wing with dynamic wingspan increased by 64.74% compared with that of fixed wingspan. After removing the influence of the area, the average thrust coefficient increased by 34.10 %.

The increments of thrust coefficient are shown in Figure 7 (right). The increments of thrust coefficient are positive during the downstroke and negative during the upstroke. It can be seen that the thrust coefficient increased during the downstroke with larger wingspan, while decreased during the upstroke with smaller wingspan.

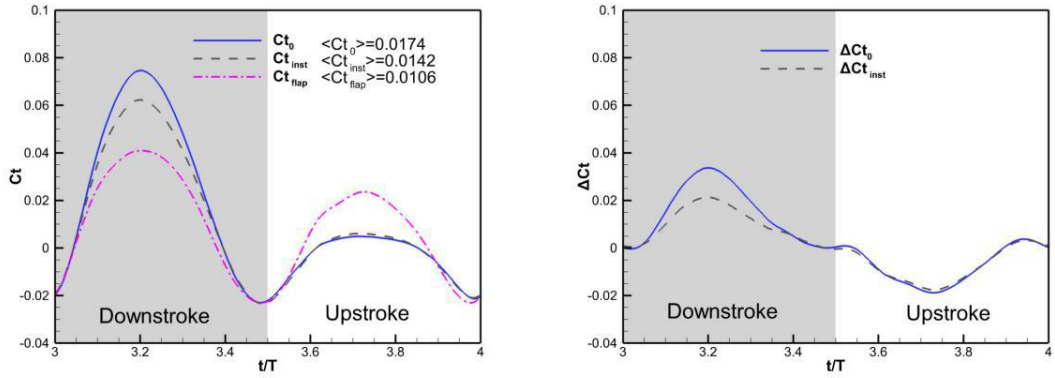

Figure 7 – Time course of thrust coefficient (left) and thrust coefficient increments (right).

3.1.2 Flow structures

To understand the physical mechanisms behind the lift enhancement associated with variable wingspan effects, the flow structures of flapping wing with dynamic wingspan and fixed wingspan are investigated. The Q-criterion is used to identify the three-dimensional (3D) vortical structures, where Q is the second invariant of the velocity gradient tensor.

The development of the unsteady flowfield around the flapping wing are shown in Figure 8, the vortical structures of flapping wing are identified with Q=500, and flooded by pressure coefficient *Cp*. The leading-edge vortex (LEV) on flapping wings is essentially a vortex sheet that increases in diameter from the wing root toward the tip. At the beginning of downstroke, the LEV emerges at the upper surface of the wing and grows along the wing-normal direction until the middle downsroke, then lifts off from the surface of the wing near the trailing edge, and eventually splits into multiple connected vortex as it approaches the end of downstroke. During the upstroke, the stress of LEV is weaker and the wingtip vortex (TV) is shedding.

The LEV of flapping wing with dynamic wingspan is intensified by the spanwise vortex stretching during the downstroke with lager wingspan, and the TV sheds more easily during the upstroke with smaller wingspan. Due to the variable wingspan effects, the intensified LEV enhanced lift of the flapping wing.

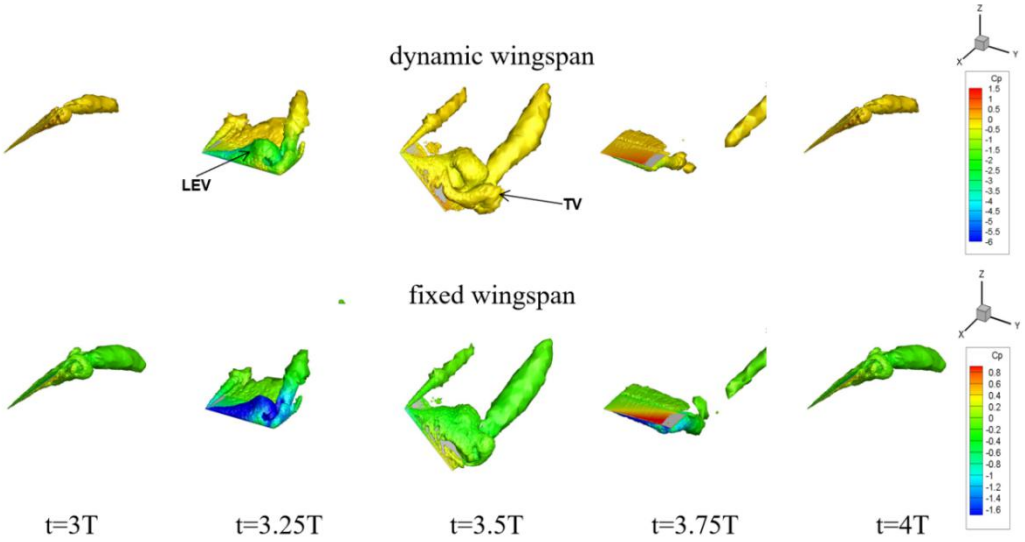

Figure 8 – The three-dimensional flow structures of flapping wing with dynamic wingspan (above) and fixed wingspan (below), the time from 3T to 3.5T is the downstroke and from 3.4T to 4T is the upstroke.

The pressure coefficient distribution on the surface of flapping wing with dynamic wingspan and fixed wingspan are similar, as shown in Figure 9. Compared with fixed wingspan, the pressure difference between upper and lower surfaces of flapping wing with dynamic wingspan is larger during the downstroke and smaller during the upstroke, which can explain the variable wingspan effects increased lift and thrust during the downstroke and decreased the thrust and negative lift during the upstroke.

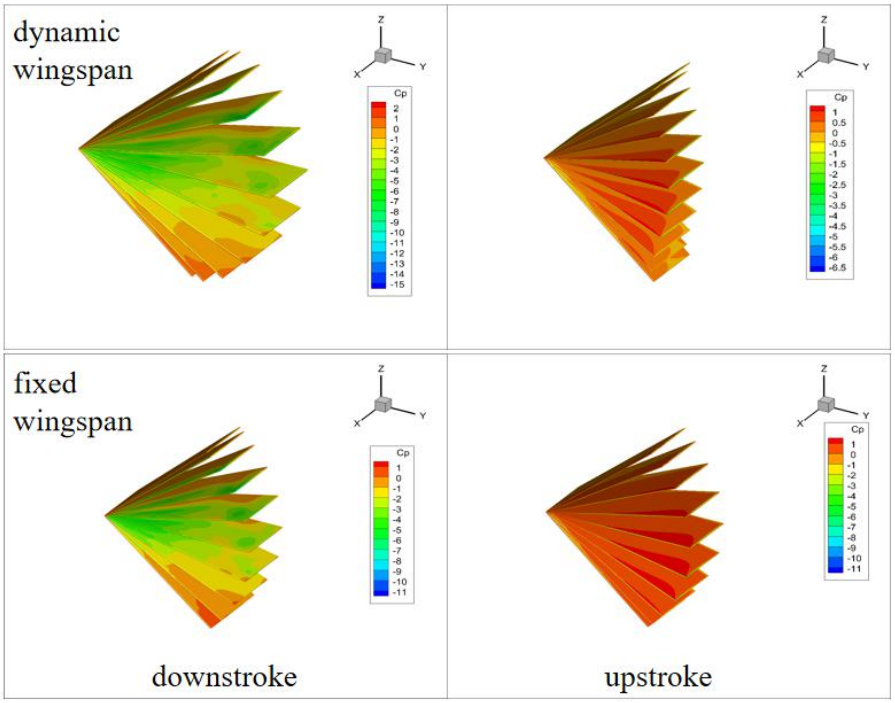

Figure 9 – The pressure coefficient distribution on the wing surface.

3.2 Aerodynamic performance respect to other parameters

3.2.1 AoA

To investigate the aerodynamic performance respect to AoA, the boundary conditions were set to U_0 = 5m/s, f = 4Hz, Ψ_m=π/4, φ = −π/2, and the AoA of the flapping wing at 5°, 10°, 15° were calculated respectively.

As shown in Figure 10, with AoA raised from 5° to 15°, the lift coefficient of the flapping wing with dynamic wingspan and fixed wingspan are both increased. In the whole flapping cycle, the lift coefficient of the flapping wing with dynamic wingspan is always larger than that of fixed wingspan. The lift coefficient increment increased during the downstroke and decreased during the upstroke with AoA raised.

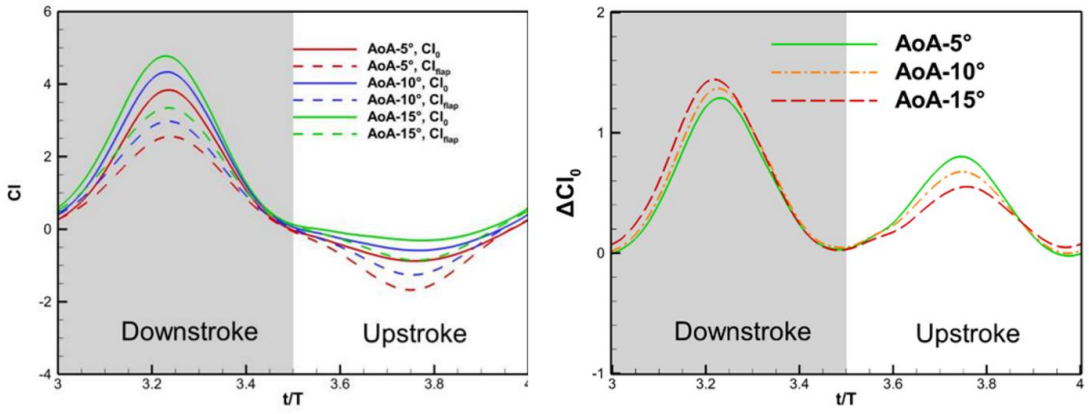

Figure 10 – Time courses of lift coefficient and lift coefficient increment respect to AoA.

With AoA raised from 5° to 15°, the thrust coefficient increased during the downstroke and decreased during the upstroke. Moreover, compared with fixed wingspan, the thrust coefficient of

the flapping wing with dynamic wingspan is larger during the downstroke and smaller during the upstroke. The thrust coefficient increment increased in the whole flapping cycle with AoA raised.

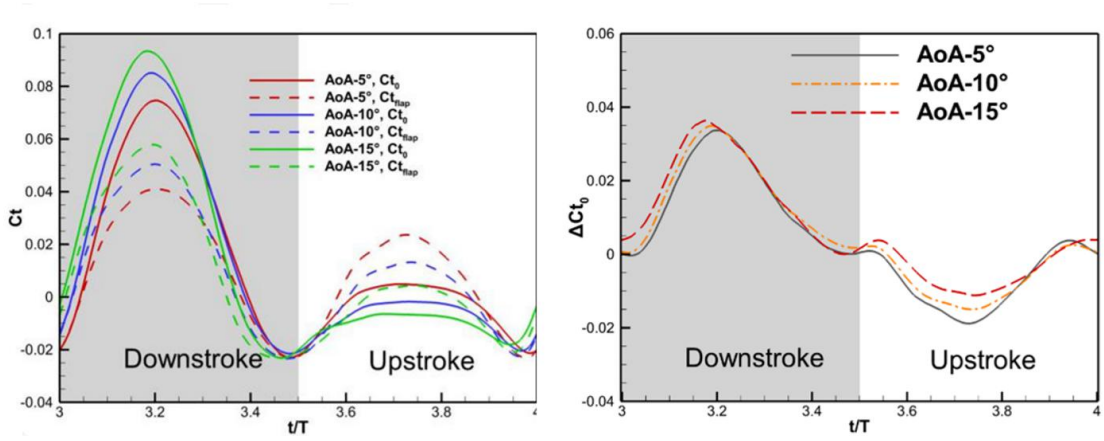

Figure 11 – Time courses of thrust coefficient and thrust coefficient increment respect to AoA.

3.2.2 Flight speed

To investigate the aerodynamic performance respect to the flight speed, the boundary conditions were set to α_0=5°, f = 4Hz, Ψ_m=π/4, φ = −π/2, and the flight speed at 5m/s, 8m/s, 11m/s were calculated respectively.

As shown in Figure 12, with the flight speed raised from 5m/s to 11m/s, the lift of the flapping wing with dynamic wingspan and fixed wingspan are both increased, while the thrusts of the flapping wings are decreased. Moreover, compared with fixed wingspan, the thrust of the flapping wing with dynamic wingspan seems larger during the downstroke and smaller during the upstroke.

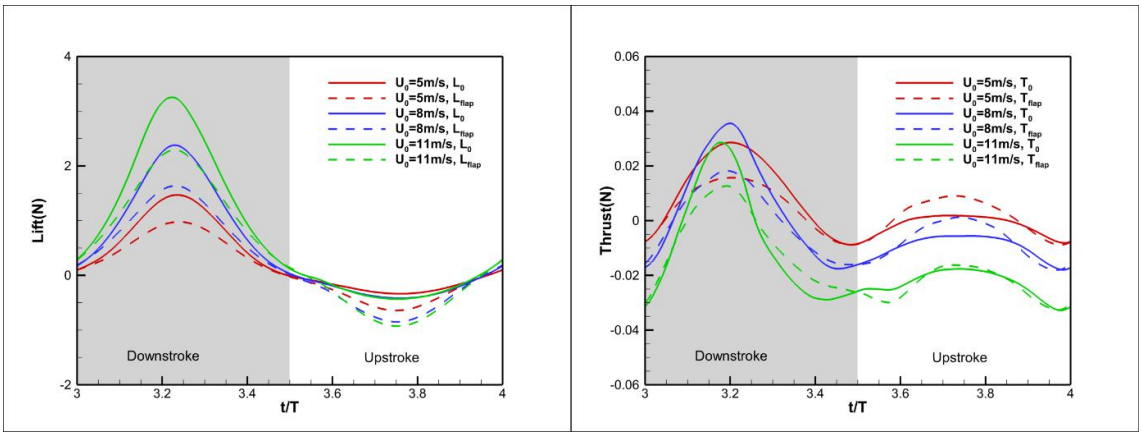

Figure 12 – Time courses of lift and thrust respect to flight speed.

With the flight speed raised from 5m/s to 11m/s, the lift coefficient and lift coefficient increment of the flapping wing reduced in the whole cycle, as shown in Figure 13. Compared with fixed wingspan, the lift coefficient of the flapping wing with dynamic wingspan is larger in the whole flapping cycle.

The thrust coefficient reduced in the whole flapping cycle with the flight speed raised. Compared with fixed wingspan, the thrust coefficient of the flapping wing with dynamic wingspan is larger during the downstroke and smaller during the upstroke. The thrust coefficient increment reduced during the downstroke and increased during the upstroke with the flight speed raised, as shown in Figure 14.

We can learn from Eqs. (4) and (13) that St and α_{eff} reduced with the flight speed raised, which may lead to the decrease of lift coefficient and thrust coefficient of the flapping wing.

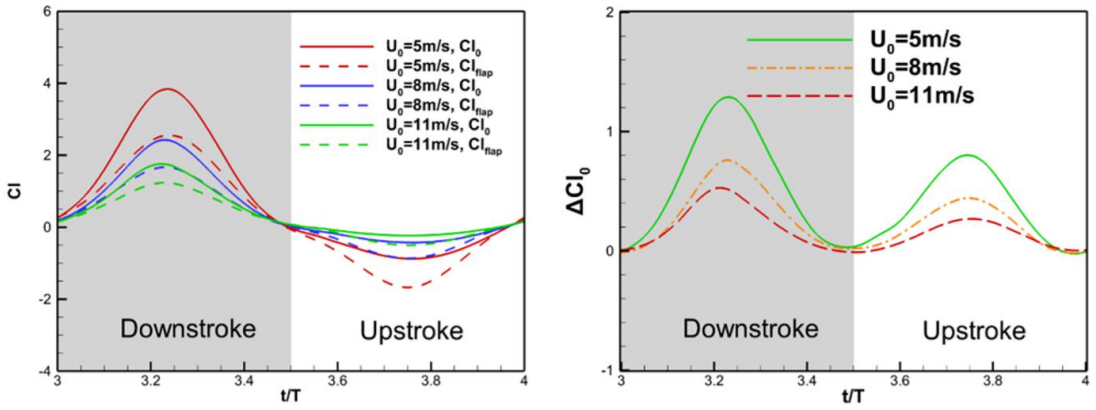

Figure 13 – Time courses of lift coefficient and lift coefficient increment respect to flight speed.

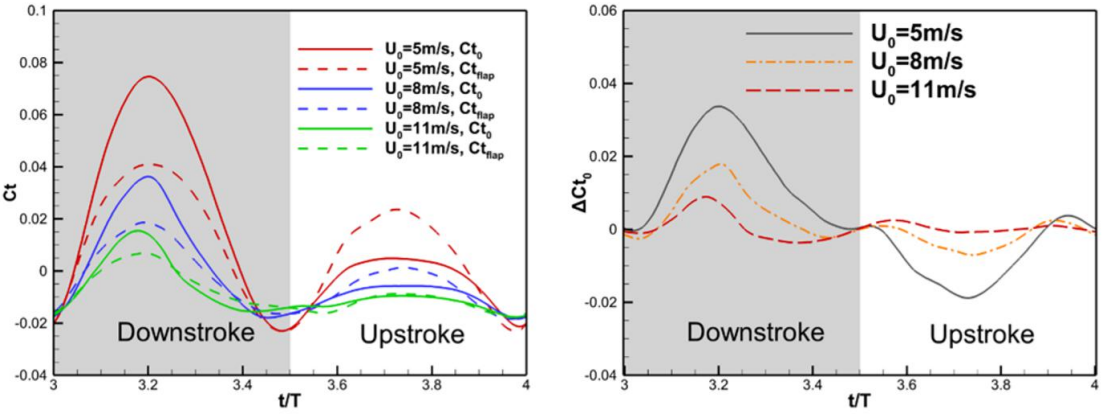

Figure 14 – Time courses of thrust coefficient and thrust coefficient increment respect to flight speed.

3.2.3 Flapping frequency

To investigate the aerodynamic performance respect to the flapping frequency, the boundary conditions were set to U_0 = 5m/s, α_0=5°, Ψ_m=π/4, φ = −π/2, and the flapping frequency at 4Hz, 6Hz, 8Hz were calculated respectively.

As shown in Figure 15, with the flapping frequency raised from 4Hz to 8Hz, the lift coefficient of the flapping wing with dynamic wingspan and fixed wingspan are both increased significantly. In the whole flapping cycle, the lift coefficient of the flapping wing with dynamic wingspan is always larger than that of fixed wingspan. The lift coefficient increment increased in the flapping cycle with the flapping frequency raised.

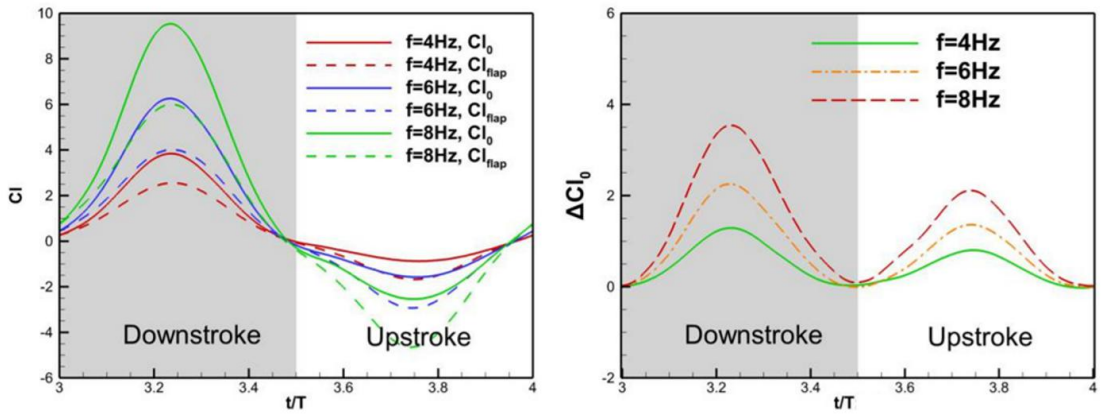

Figure 15 – Time courses of lift coefficient and lift coefficient increment respect to the flapping frequency.

With the flapping frequency raised from 4Hz to 8Hz, the thrust coefficient of the flapping wing with dynamic wingspan and fixed wingspan are both increased significantly, as shown in Figure 16. Compared with fixed wingspan, the thrust coefficient of the flapping wing with dynamic wingspan is larger during the downstroke and smaller during the upstroke. The lift coefficient increment increased during the downstroke and reduced during the upstroke with the flapping frequency raised.

We can learn from Eqs. (4) and (13) that St and α_{eff} increased with the flapping frequency raised, which may lead to the increase of lift coefficient and thrust coefficient of the flapping wing.

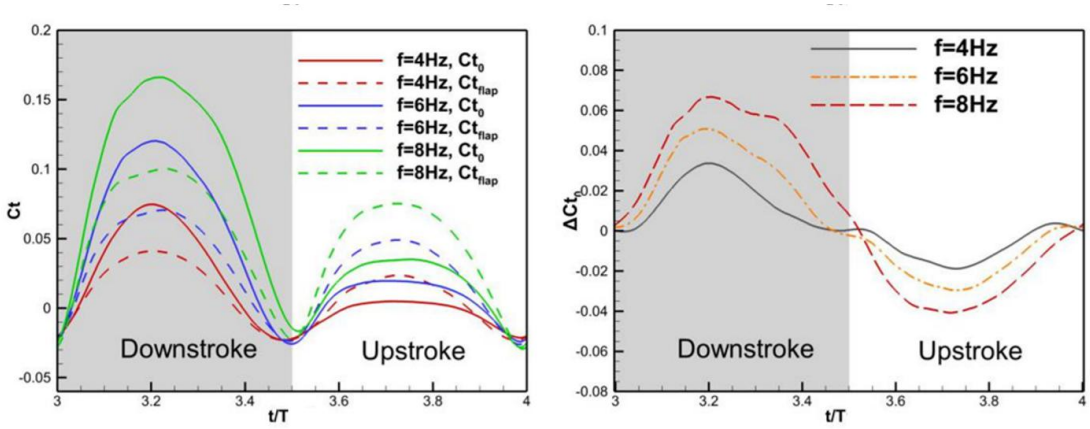

Figure 16 – Time courses of thrust coefficient and thrust coefficient increment respect to the flapping frequency.

4. Conclusions

In this research, the flapping wing with variable wingspan are simulated and compared with fixed wingspan. The aerodynamic characteristics and evolution of vortex structure between these two kinds of wings are compared and analyzed. In the whole flapping cycle, the increments of lift coefficients generated by variable wingspan are positive, and the averaged lift coefficient nearly double compared with fixed wingspan. The thrust coefficient increases during the downstroke because of the larger wingspan, while reduces during the upstroke because of the smaller wingspan. The LEV of flapping wing with dynamic wingspan is intensified by the spanwise vortex stretching during the downstroke with lager wingspan, which can enhance the lift coefficient of the flapping wing. In extensive flight conditions, the lift coefficient and thrust coefficient are increased due to the variable wingspan effects, which can significantly improve the aerodynamic performance of the flapping wing. The flapping wing with dynamic wingspan can be used in FMAVs to improve the flight performance.

5. Contact Author Email Address

Mail to: zhangrui1840@mail.nwpu.edu.cn

6. Copyright Statement

7. Acknowledgments

This study was supported by the National Natural Science Foundation of China (11872314) and the Key R&D Program in Shaanxi Province of China (2020GY-154).

References

[1] LI Zhanke, SONG Bifeng , SONG Hailong. Study on actualities of micro air vehicles and its key technologies. Flight Dynamics.2003(04): 1-4[Chinese].

[2] Yang Wenqing, Song Bifeng, Gao Guanglin. Flight performance estimation of bionic flapping-wing micro air vehicle.Journal of Northwestern Polytechnical University. 2018, 36(04): 636-643[Chinese].

[3] Ramezani A, Chung S J, Hutchinson S. A biomimetic robotic platform to study flight specializations of bats[J]. Sci. Robot., 2017, 2(3): Art. No. eaal2505.

[4] Ajanic E, Feroskhan M, Mintchev S, et al. Bioinspired wing a and tail morphing extends drone flight capabilities[J]. Sci. Robot., 2020, 5: eabc2897.

[5] Chang E, Matloff L Y, Stowers A K, et al. Soft biohybrid morphing wings with feathers underactuated by wrist and finger motion[J]. Sci. Robot., 2020, 5(38).

[6] Chin D D, Matloff L Y, Stowers A K, et al. Inspiration for wing design: how forelimb specialization enables active flight in modern vertebrates[J]. Journal of the Royal Society Interface, 2017, 14(131): 20170240.

[7] Shyy W, Aono H, Chimakurthi S K, et al. Recent progress in flapping wing aerodynamics and aeroelasticity[J]. Progress in Aerospace Sciences, 2010, 46(7): 284-327.

[8] Jantzen R T, Taira K, Granlund K O, et al. Vortex dynamics around pitching plates[J]. Physics of Fluids, 2014, 26(5): 53606.

[9] Krishna S, Green M A, Mulleners K. Flowfield and force evolution for a symmetric hovering flat-plate wing[J]. AIAA Journal, 2018, 56(4): 1360-1371.

[10]WANG S, ZHANG X, HE G, et al. Lift enhancement by dynamically changing wingspan in forward flapping flight[J]. Physics of Fluids, 2014, 26(6): 61903.

[11]Krishna, Swathi, Melissa A. Green, and Karen Mulleners. "Flowfield and force evolution for a symmetric hovering flat-plate wing." AIAA Journal 56.4 (2018): 1360-1371.

[12]Z.W. Guan, Y.L. Yu, Aerodynamic mechanism of forces generated by twisting model-wing in bat flapping flight, Appl. Math. Mech. (English Ed.) 35 (2014):1607–1618.

[13]Yu, Yongliang, and Ziwu Guan. "Learning from bat: aerodynamics of actively morphing wing." Theoretical and Applied Mechanics Letters 5.1 (2015): 13-15.

[14]Heathcote S, Wang Z, Gursul I. Effect of spanwise flexibility on flapping wing propulsion[J]. Journal of Fluids and Structures, 2008, 24(2): 183-199.

[15]LIU H. Integrated modeling of insect flight: From morphology, kinematics to aerodynamics[J]. Journal of Computational Physics, 2009, 228(2): 439-459.